Published in final edited form as:
J Endocrinol. 2009 July ; 202(1): 17–28. doi:10.1677/JOE-09-0079.

A new mouse model of metabolic syndrome and associated complications

Yun Wang, **Yue Zheng**, **Patsy M Nishina**, and **Jürgen K. Naggert**
The Jackson Laboratory, 600 Main Street, Bar Harbor, ME, 04609

Abstract

Metabolic Syndrome (MS) encompasses a clustering of risk factors for cardiovascular disease, including obesity, insulin resistance, and dyslipidemia. We characterized a new mouse model carrying a dominant mutation, C57BL/6J-*Nmf15*/+ (B6-*Nmf15*/+), which develops additional complications of MS such as adipose tissue inflammation and cardiomyopathy.

A backcross was used to genetically map the *Nmf15* locus. Mice were examined in the CLAMS™ animal monitoring system, and dual energy X-ray absorptiometry and blood chemistry analyses were performed. Hypothalamic LepR, SOCS1 and STAT3 phosphorylation were examined. Cardiac function was assessed by Echo- and Electro Cardiography. Adipose tissue inflammation was characterized by in situ hybridization and measurement of Jun kinase activity.

The *Nmf15* locus mapped to distal mouse chromosome 5 with a LOD score of 13.8. *Nmf15* mice developed obesity by 12 weeks of age. Plasma leptin levels were significantly elevated in pre-obese *Nmf15* mice at 8 weeks of age and an attenuated STAT3 phosphorylation in the hypothalamus suggests a primary leptin resistance. Adipose tissue from *Nmf15* mice showed a remarkable degree of inflammation and macrophage infiltration as indicated by expression of the F4/80 marker and increased phosphorylation of JNK1/2. Lipidosis was observed in tubular epithelial cells and glomeruli of the kidney. *Nmf15* mice demonstrate both histological and pathophysiological evidence of cardiomyopathy.

The *Nmf15* mouse model provides a new entry point into pathways mediating leptin resistance and obesity. It is one of few models that combine many aspects of metabolic syndrome and can be useful for testing new therapeutic approaches for combating obesity complications, particularly cardiomyopathy.

Keywords

mouse model; hyperleptinemic obesity; adipose inflammation; renal lipidosis; cardiomyopathy; metabolic syndrome

Introduction

The term “metabolic syndrome” (MS) is used to describe the simultaneous occurrence of obesity, insulin resistance, dyslipidemia, and hypertension. This syndrome is emerging as one of the major medical and public health problems both in the United States and worldwide.

Address correspondence to: Jürgen K Naggert Ph.D. The Jackson Laboratory, 600 Main Street, Bar Harbor, ME Tel.: 207-288-6382. Fax: 207-288-6077; Juergen.Naggert@jax.org.

There is no conflict of interest among authors that would prejudice the impartiality of this work.

Currently, approximately 25% of North Americans are thought to be affected by metabolic syndrome (Eckel, et al. 2005; Tiffin, et al. 2008). As the epidemic of obesity shows no signs of reversing, the prevalence of the MS is likely to rise in the future (Ford, et al. 2002). Despite its high prevalence, the pathogenesis of MS is not completely understood (Olufadi and Byrne 2008).

Although existing mouse models have been fundamental to advancing our knowledge of the basis of obesity, type 2 diabetes, and dyslipidemia, we are still at an early stage in understanding MS as a complex disorder. Traditionally, leptin-deficient (*Lep* ^{ob}) and leptin receptor-deficient (*Lepr*^{db}) mice, representing extremes of obesity syndromes, have been used for studies of obesity, adipocyte dysfunction, and insulin resistance (Coleman 1985). More recently, diet induced and polygenic models have become increasingly used, but pose challenges for the identification of the underlying genetic causes of their phenotypes. Therefore, there remains a need for new monogenic animal models that recapitulate the complexity of the human metabolic syndrome. The study of two aspects of metabolic syndrome in particular would benefit from the availability of new models, adipose tissue inflammation and obesity associated cardiomyopathy.

Obesity-induced inflammation is characterized in part by the infiltration of macrophages and other immune cells into white adipose tissue (WAT) and has been observed in both rodents and humans (Cancello and Clement 2006; Wellen and Hotamisligil 2003). However, the molecular reasons for adipose tissue inflammation and macrophage infiltration in obesity is not fully understood (Heilbronn and Campbell 2008).

Most reports of cardiac dysfunction have used type 1 diabetes-induced (T1D) models (Tomlinson, et al. 1992; Yu, et al. 1994), whose usefulness with respect to metabolic syndrome may be limited to hyperglycemia. Non-insulin-dependent (type 2) diabetes is a prevalent disease that results in an increase in cardiovascular complications (Grundy, et al. 1999) among them a specific cardiomyopathy, characterized by ventricular dysfunction in the absence of atherosclerotic coronary heart disease or hypertension (Fein 1990).

The *Nmf15* mouse model carries a dominant mutation generated through ENU mutagenesis. As reported herein, mice heterozygous for the *Nmf15* mutation phenotypically develop late onset obesity. In addition to obesity, dyslipidemia, and adipose tissue inflammation, B6-*Nmf15*/+ mice are also characterized by hyperinsulinemia without significant hyperglycemia. Hyperleptinemia is already found in young pre-obese mice (7–8 weeks of age) fed standard chow. In addition, B6-*Nmf15*/+ mice develop lipid deposits in liver and kidney, and a progressive dilated cardiomyopathy (DCM). The unique combination of features in *Nmf15* mice offers a useful paradigm for understanding human hyperleptinemic metabolic syndromes associated with obesity and cardiac failure. Since the MS in *Nmf15* mice is a single gene trait, the underlying genetic cause is more easily tractable and will lead to the identification of a critical component in the disease pathway leading to MS. *Nmf15* mice also represent a valuable new tool for testing new therapies.

Materials and methods

Mice

Breeding pairs of B6-*Nmf15*/+ mice were obtained from the Neuro Mutagenesis Facility at The Jackson Laboratory. Colonies of *Nmf15* mice were maintained on a NIH mouse/rat diet with 4% fat (#5K54, PMI Feeds Inc., St. Louis, MO), fed ad libitum with free access to water (HCl acidified, pH 2.8–3.2) under controlled temperature and humidity with a 12-hour light and dark cycle (lights on from 6:00–18:00 hrs). All animal studies were performed with the approval of The Jackson Laboratory Animal Care and Use Committee (protocol no. 99089).

Transfer of the Nmf15 mutation onto a non-mutagenized C57BL/6J background—To reduce the mutation load that is present in mutant mice obtained from an ENU mutagenesis screen, the mutant C57BL/6J-*Nmf15*/+ (B6-*Nmf15*/+) mice were backcrossed to non-mutagenized C57BL/6J (B6) mice. To characterize the dominant MS mutation, B6-*Nmf15*/+ mice beyond backcross generation 7 (>N7) were used.

Inheritance of Nmf15—An obese mouse (*Nmf15*) was observed in the first generation (G1) of an ENU mutagenesis screen. Breeding of the founder mouse to wt B6 confirmed that the obesity phenotype was inherited as a dominant trait. Despite several attempts either through intercrossing of B6.AKR-*Nmf15*/+ mice or by ovarian transplant, no mice homozygous for the *Nmf15* mutation were obtained.

Chromosomal mapping of the Nmf15 mutation—We conducted a genome-wide mapping study for obesity in B6-*Nmf15*/+ mice by out-crossing to the inbred AKR/J strain mice and backcrossing male and female (AKR × B6-*Nmf15*/+) F1 mice to AKR/J. A cohort of backcross (BC) mice from the cross was genotyped and phenotyped for body weight at 12 weeks of age. Thirty-five BC animals were genotyped using 57 evenly spaced microsatellite markers for a genome scan to locate the *Nmf15* mutation. The location was confirmed and the map position refined in a second cohort of 239 BC animals genotyped using 11 microsatellite markers on chromosome 5. Isolation of genomic DNA and genotyping were described previously (Wang, et al. 1997).

QTL mapping and statistics

QTL analysis and genome scans were performed using the scanone and bayesint functions of the R/qtl package (http://research.jax.org/faculty/churchill/software/Jqtl/index.html) as described previously (Broman, et al. 2003). Significance of QTL LOD scores was assessed using 1000 permutations of the phenotypic data (Churchill and Doerge 1994). A Bayesian credible interval for chromosome 5 was computed and reported as confidence interval.

Comprehensive laboratory animal monitoring system (CLAMS™)

The Comprehensive Laboratory Animal Monitoring System (CLAMS™, Columbus Instruments, Columbus, OH) is a set of live-in cages for automated, non-invasive and simultaneous monitoring of horizontal and vertical activity, feeding and drinking, oxygen consumption and CO_2 production. Seven to eight-week-old B6-*Nmf15*/+ mice and controls were individually placed in CLAMS™ cages and monitored over a 5-day period. Food and water consumption are measured directly as accumulated data. The hourly file displays all measurements for each parameter: VO_2 (volume of oxygen consumed, mL/Kg/hr), VCO_2 (volume of carbon dioxide produced, mL/Kg/hr), RER (respiratory exchange ratio), heat (Kcal/hr), accumulated food (grams), accumulated drink (grams), XY total activity (all horizontal beam breaks in counts), XY ambulatory activity (minimum 3 different, consecutive horizontal beam breaks in counts) and Z activity (all vertical beam breaks in counts). The data were recorded during the 30-second sampling period.

Dual energy X-ray absorptiometry (DEXA)

The LUNAR PIXImus mouse densitometer (GE Lunar, Madison, WI) is a dual-energy supply X-ray machine for measuring skeletal and soft tissue mass, enabling assessment of skeletal and body composition in mice. Mice scanned alive were anesthetized with 2% tribromoethanol. Mice were individually placed on plastic trays, which were then placed onto the exposure platform of the PIXImus machine to measure body composition.

Metabolic parameters and glucose homeostasis

Blood was drawn approximately 4 hours after the onset of light from the retro-orbital plexus via heparinized capillary tubes and plasma was obtained by centrifugation (1200×g) at 4 °C. Measurements of plasma glucose, total-cholesterol, HDL- and LDL-cholesterol, triglycerides, free fatty acids, alkaline phosphatase, pancreatic lipase, T4, and calcium were performed using a Beckman Coulter Synchron CX5 Delta chemistry analyzer (Beckman Coulter, Inc., Diagnostic Division, Brea, CA, USA). The plasma hormone levels of leptin, adiponectin, resistin and insulin were measured by ELISA (Linco Research, St. Charles, MO, USA).

For the glucose tolerance test (GTT), mice were fasted for 16 hours, and were given intraperitoneal injection with 0.5 g/kg dosage (50% solution of D-50 Dextrose). Blood glucose levels were measured using OneTouch Ultra Blood Glucose Monitoring system at 15, 30, 60, 120 and 180 minutes after glucose administration. For insulin tolerance tests (ITT), mice were fasted for up to 4 hours and the insulin diluted in 0.9% saline was administered by IP injection (1U/kg). Blood glucose levels were monitored as above immediately prior to injection T_0, and at 30, 60, 90, and 120 minutes after injection. These data were expressed as % T_0 blood glucose levels vs. time.

Real-time quantitative PCR

Real-time PCR assays were performed as previously described (Wang, et al. 2006) on an ABI PRISM 7500 SDS instrument. Samples were analyzed in triplicate in three independent runs. To quantify the gene expression profiles, we used the comparative threshold cycle method. PCR amplified 150–180 bp fragments of cDNA, IL-6 (F: GCTAAGGACCAAGACCATCCAAT, R: CTTGAACATAAGACAGATAGGACCAA), MCP-1 (FACTGCATCTGCCCTAAGGTCTT, R: GTGCTTGAGGTGGTTGTGGAA), PAI-1 (F: GGCCAAAGGAAAAAGCACTGT, R: GGGCCACCATTTGATCTGTCTA), and TNF-a (F: GACGTGGAACTGGCAGAAGAG, R: GCCACAAGCAGGAATGAGAAG).

Histopathology of the heart, liver, and kidney

Tissues of B6-*Nmf15*/+ mice and age-matched littermate controls were harvested, washed with ice-cold PBS, and either fixed in 10% formalin or in Streck's tissue fixative (Streck Laboratories, Omaha, Neb.) overnight and were finally paraffin-embedded. Histochemical analysis was carried out on 4-μm-thick sections using Haematoxylin and Eosin (H.E.) and trichrome staining.

Oil red-O staining

Frozen 10-μm-thickness cryosections from liver and kidney were fixed with 10% formaldehyde. Approximately 5 min after the fixation, Oil-Red O stain (Oil Red O stock solution saturated in isopropanol, Rowley Biochemical Institute, cat: So-385) was used for 10 min to stain for lipid accumulation. After rinsing with distilled water, the slides were stained in Mayers Hematoxylin for 5 minutes, washed with distilled water for 15 minutes and mounted with aqueous solution. Sections were visualized at a magnification of ×40 and ×100.

Echocardiography (Echo)

Vevo 770 High-Frequency Ultrasound equipment (Visualsonics, Toronto, Ontario, Canada) was used. Animals were anesthetized with 5% isoflurane at 0.8 l/min and maintained anesthetized with 1–1.5% isoflurane at 0.8 l/min. Animals were allowed to recover under a heat lamp upon completion of imaging.

Electrocardiogram (ECG)

The animals were restrained in a Murine ECG Restrainer from QRS Phenotyping Inc., Calgary, Alberta, and the signal acquisition used a PowerLab system from AD Instruments, Golden CO. To perform an electrocardiogram (ECG) on anesthetized mice, the animals were anesthetized with 5% isoflurane at 1 l/min and maintained at 1.5% at 0.8 l/min. Body temperature was maintained with an overhead heat lamp. A three-lead configuration was used to acquire the electrical signals.

Measurement of blood pressure (BP)

The CODA6 non-invasive blood pressure system (Kent Scientific Torrington, CT USA) was used to measure blood pressure parameters: systolic, diastolic, mean, heart pulse rate, tail blood volume, and tail blood flow. Mice were placed in a clear plastic tube with nose cone and tail hole pieces secured at either end. These tubes were then placed on a platform heated to ~35° C and the mice were allowed to warm to platform temperature for 5–15 minutes prior to the experiment. Mice were habituated to the procedure with 10–30 preliminary cycles; thereafter 30 data measurements were recorded for each mouse. Measurements were performed at the same time each day, generally between 7 and 11am in a sound-barrier room.

In situ hybridization

Adipose tissue was fixed in 4% paraformaldehyde PBS for 18 hours, dehydrated, and embedded in paraffin. A minimum of three samples from three different animals in each group were used for this experiment. Sections of 6-μm thickness were cut and mounted on slides pretreated with poly L-lysine (Sigma, St. Louis, MO). The sense and antisense riboprobes were generated from plasmids containing cDNA fragments of F4/80 labeled by digoxigenin (DIG).

Measurement of JNK activation

The phosphorylation status at threonine 183 and tyrosine 185 of JNK1/2 was assayed using a commercial antibody bead kit for phospho-JNK1/2 [pTpY 183/185] (Cat. LHO0081, Biosource, Camarillo, CA).

Western blot analysis

After an over night fast, mice were injected with saline or leptin intraperitoneally (IP) (3 mg/kg). Five hours later, mice were anesthetized before decapitation, and the brain was rapidly removed (Martin, et al. 2006). Using a cooled mouse brain matrix with 1-mm section dividers, the hypothalamus was dissected as described previously (Martin et al. 2006) (Munzberg, et al. 2004). Hypothalamus tissue lysates were prepared as described previously (Martin et al. 2006). Phosphorylation of STAT3 in the hypothalamus was determined by western blot analysis of a 4–12% SDS-acrylamide gels using an antibody against phosphotyrosine705 (Cell Signaling) of STAT3 (Cell Signaling). The measurements of phosphorylation of JKN1/2 in adipose tissue and LepR and SOCS1 in the hypothalamus were carried out by western blot analysis of 10% SDS-acrylamide gels using antibodies against phosphorylated JKN1/2 (Cell Signaling), LepR (Santa Cruz) and SOCS1 (Abcam), respectively.

Statistical analysis

Values are expressed as mean ± S.E.M. All groups of animals were studied in parallel. Comparisons between different groups were performed by Student's t-test for unpaired samples. The level of significance was $P<0.05$.

Results

Mapping of the Nmf15 locus

To genetically map the *Nmf15* mutation, mutant mice were outcrossed to the strain AKR/J and the F1 generation backcrossed to AKR/J to produce a mapping panel. Twelve-week bodyweight was used as a quantitative trait (Figure 1A). We initially mapped the body weight trait to chromosome 5 with a suggestive LOD score of 2.25 (Figure 1B). To confirm and refine the map position, a second backcross cohort was analyzed using additional, more closely spaced markers on chromosome 5. The *Nmf15* map position was confirmed with a peak LOD score of 13.8 on distal chromosome 5. The 95% confidence interval was between 44 cM and 60 cM (Figure 1C).

B6-Nmf15/+ mice are obese and have decreased activity levels and reduced oxygen consumption

Bodyweight and body composition from dominant obese B6-*Nmf15*/+ mice were measured. The body weight changes in B6-+/+ and B6-*Nmf15*/+ mice from 4 to 20 weeks of age are shown in Figure 2A. At 12 weeks of age, B6-*Nmf15*/+ mice are heavier than controls (female: 32 ± 4.6 vs 24 ± 1.8; male: 35 ± 3.5 vs 27 ± 2.5). This increase was exclusively due to an increase in body fat, since lean body mass was not different in B6-*Nmf15*/+ mice compared with their littermates at 12-14-week of age. The body fat gain of B6-*Nmf15*/+ mice was more than three times higher (15.2g) than that of control mice (5.2g), (Figure 2B and C).

B6-*Nmf15*/+ and control mice at 8 weeks of age (pre-obese) were housed in the comprehensive laboratory animal monitoring system (CLAMS™). All animals were single-housed in the metabolic cages over a 5-day period for collection of data. Only the last three-day period was analyzed to reduce variation introduced by adapting to a new environment. Figure 2 shows the daily patterns of metabolic measurements. Total locomotor activity was reduced (Figure 2D), and the overall food intake was the same in B6-*Nmf15*/+ mice compared to littermate controls, indicating that B6-*Nmf15*/+ mice are not hyperphagic (Figure 2E). There was decreased consumption of oxygen (Figure 2F) during dark and light periods, perhaps reflecting the reduced activity levels. The respiratory quotient, indicative of macronutrient utilization was not different between B6-*Nmf15*/+ mice and littermate controls (data not shown).

B6-Nmf15/+ mice are hyperleptinemic and show reduced leptin sensitivity in the hypothalamus

A panel of immunoassays for mouse adipokines was used to profile longitudinal changes in B6-*Nmf15*/+ mice between 8 and 32 weeks of age (Figure 3A and B). Both female and male B6-*Nmf15*/+ mice at 8 weeks did not show a significant difference in body weight and body fat compared with their controls (Figure 2A). However, leptin levels were already significantly elevated in young pre-obese B6-*Nmf15*/+ mice (13,560±4,600 vs. 2,300±447, $p<0.005$) (Figure 3A). Circulating adiponectin levels in B6-*Nmf15*/+ mice were slightly higher than their controls at 8 and 16 weeks, but not different by 32 wks of age (Figure 3B). There was no difference in the levels of resistin between B6-*Nmf15*/+ mice and normal littermates (data not shown).

To assess whether the high leptin levels in *Nmf15* mice may be caused by leptin resistance, the hypothalamic protein levels of LepR and SOCS1were determined. Increased levels of Leptin receptor (2.5 fold) and SOCS1 (1.35 fold) were observed in *Nmf15* mice compared to their controls (Figure 3C and D). We also measured STAT3 activation in the hypothalamus. In our study, STAT3 phosphorylation was increased 1.7 fold in control mice after leptin stimulation, but was not significantly increased in *Nmf15* mice (Figure 3E).

B6-Nmf15 mice have impaired glucose metabolism

Table 1 shows baseline data for blood constituents in 20–25 week-old male B6-*Nmf15*/+ mice. No differences were detected in plasma glucose, but hyperinsulinemia was observed in male B6-*Nmf15*/+ mice from 16 weeks of age (Figure 4A). There were elevated levels in triglyceride (143±3.8 vs.95.3±7.5 mg/dL, P<0.03) and free fatty acid (4.72±0.5 vs. 3.4±0.3 mEq/L, P<0.05) between B6-*Nmf15*/+ mice and normal littermates (Table 1). *Nmf15* mice exhibited impaired glucose tolerance (Figure 4C), and these m ice were unresponsive to exogenous insulin during an insulin tolerance test (Figure 4B), indicating marked insulin resistance.

B6-Nmf15/+ obese mice develop cardiomyopathy, renal lipidosis and adipose tissue inflammation

B6-*Nmf15*/+ mice also demonstrate both histological and pathophysiological evidence of cardiomyopathy. Histological analysis revealed that hearts from 20-week-old B6-*Nmf15*/+ mice displayed distinguishable chamber dilation and decreased thickness of the ventricular wall (Figure 5B) in comparison to their controls (Figure 5A). To characterize the disease phenotype, we conducted echocardiography to assess global cardiac function in B6-*Nmf15*/+ mice in comparison with age-matched littermate controls. Echocardiography (echo) demonstrated that left ventricular ejection fraction (LV EF), left ventricular shortening (LV ES) and cardiac output were reduced and the LV cavity was dilated in B6-*Nmf15*/+ mice at 20 weeks of age (Table 2). There was a tendency toward lower blood pressure (106±22 vs 95±24/ mmHg) and a significant decrease in pulse rate (711±15.7 vs 652±13.9, p<0.05/ beats/min) in B6-*Nmf15*/+ mice at 12–16 weeks of age (Figure 5E and F). Livers from B6-*Nmf15*/+ animals exhibited a classical “nutmeg” appearance with dark red areas of central venous congestion (Figure 5D). Long-standing chronic passive congestion of the liver is characterized by congested parenchyma around the central veins surrounded by paler peripheral tissue. Nutmeg liver is thought to be caused by chronic passive congestion of the liver secondary to heart failure (Kawase, et al. 2002).

Lipid deposits have been observed in multiple tissues in obese B6-*Nmf15*/+ mice. Kidney vacuolizations were found in B6-*Nmf15*/+ mice at 20–25 weeks age. Vacuoles were present in proximal tubule epithelial cells and proteinaceous material accumulated in the tubules (Figure 6B). Signs of glomerulosclerosis were also observed in the kidney of B6-*Nmf15*/+ mice (Figure 6B, D and F). Frozen sections of the kidney from B6-*Nmf15*/+ mice were strongly stained by Oil-red-O for lipid in tubular epithelial cells (Figure 6D) and in glomeruli (Figure 6F). Staining for lipid on frozen sections from the littermate controls yielded negative results. The livers in both male and female B6-*Nmf15*/+ mice were significantly larger than those of their littermate controls. The macro- and micro-vesicular lipid deposits using H&E staining and Oil Red-O frozen staining revealed remarkable hepatosteatosis in B6-*Nmf15*/+ mice (Figure 6H and L).

Adipose tissue from B6-*Nmf15*/+ mice showed a remarkable degree of inflammation and macrophage infiltration. Histological analyses revealed mononuclear infiltrates in white adipose tissue from B6-*Nmf15*/+ mice. The majority of infiltrating cells were macrophages (Figure 7 B and D), as in situ hybridization assays demonstrated that they expressed the macrophage specific marker F4/80 (Figure 7D). Activation of JUN N-terminal kinase (JNK, now called MAPK8) has been associated with obesity-induced inflammation in adipose tissue (Solinas, et al. 2007). We analyzed JNK1/2 phosphorylation in protein extracts from adipose tissue of B6-*Nmf15*/+ mice and controls. As shown in Figure 7E, JNK phosporylation was enhanced 2 fold in B6-*Nmf15*/+ mice compared with their controls. Furthermore, we measured the protein and phosphorylation levels of JNK in B6-*Nmf15*/+ mice by western blotting. Phosphorylation of JNK in adipose tissue of B6-*Nmf15*/+ mice was significantly increased compared to controls (Figure 7F). Adipose tissue is an important endocrine organ producing

various cytokines that are involved in inflammatory pathways, such as IL-6, TNF-α, MCP-1, and PAI-1 (Kershaw and Flier 2004). Adipose cytokine gene expression levels (IL-6, TNF-α, MCP-1, and PAI-1) in adipose tissue of B6-*Nmf15*/+ mice were all significantly higher than in controls (Figure 7G).

Discussion

The metabolic syndrome is a cluster of metabolic abnormalities, including obesity, insulin resistance, and dyslipidemia, which individually and collectively are major risk factors for cardiovascular disease. More recently it has been proposed that an inflammatory state induced by obesity may underlie many of these risk factors (Rana, et al. 2007). Here we describe a new mouse model of obesity, *Nmf15*, which combines several of the features and complications of human metabolic syndrome, including adipose tissue inflammation and cardiomyopathy.

A genome-wide scan using microsatellite markers was carried out and the *Nmf15* mutation was mapped to distal chromosome 5. No previously mapped genes in this area have been associated with obesity or leptin signaling. However, QTL affecting body weight in four different crosses have been mapped to the same region (Brockmann, et al. 2000) (Togawa, et al. 2006). Potential candidate genes in the region include thyroid hormone receptor associated protein 2 (*Med13l*), neuropeptide FF receptor 2 (*Npffr2*), G-coupled protein receptor 81 (*Gpr81*), and carbohydrate response element binding protein (*Mlxipl*). Analysis of the cDNA of these genes did not detect any sequence variation. The *Nmf15* locus in the distal region on mouse chromosome 5 shares conserved synteny with a region of human chromosome 7. Two studies recently reported that a novel locus for autosomal-dominant cardiomyopathy maps to this region (Schonberger, et al. 2005) (Song, et al. 2006). The *Nmf15* locus is, therefore, likely to encode a previously undiscribed signal or factor essential for the development of obesity and cardiac failure in *Nmf15* mice, or defines a previously unknown function for a known gene.

Hotamisligil et al. have demonstrated the existence of an inflammatory state involving the adipose tissue for the first time in 1993 (Hotamisligil, et al. 1993). Adipocytes are the most important source of adiponectin. A strong epidemiological relationship between low circulating adiponectin and diabetes, metabolic syndrome, and cardiovascular disease has been reported in humans (Chandran, et al. 2003),(Fantuzzi 2005). B6-*Nmf15*/+ mice showed initially increased plasma adiponectin levels compared to controls, but the levels declined later in the development of the B6-*Nmf15*/+ obesity syndrome (Figure 3F). Todoric et al (Todoric, et al. 2006) reported that high-fat diet-induced down-regulation of adiponectin gene expression in Lepr ^{db} mice was paralleled by reduced adiponectin serum concentration. NONcNZO5, a polygenic obesity syndrome mouse strain, showed a tendency for first increased and then reduced serum adiponectin levels during aging and progression of the obesity phenotype (Leiter, et al. 2007). Several reports have ascribed anti-inflammatory effects to adiponectin, including inhibition of TNF production and activity, inhibition of nuclear factor-B activation, induction of anti-inflammatory cytokines, as well as down-regulation of adhesion molecules (Wolf, et al. 2004; Yamaguchi, et al. 2008). This indicates that adiponectin may be induced as a protective response to adipose tissue inflammation. As the inflammation in B6-*Nmf15*/+ mice progresses, however, the protective mechanisms may become overwhelmed and adiponectin levels decline.

The finding that B6-*Nmf15*/+ mice are hyperleptinemic before the increase in adipose tissue mass suggests that leptin resistance underlies the observed phenotypes. This is supported by our finding that the downstream intermediate of the leptin signaling pathway, STAT3, is not phosphorylated in the hypothalamus in response to leptin stimulation in *Nmf15* mice as it is in control B6 mice. Obese rodents, and humans, are resistant to leptin, in some cases because of genetic disposition (primary resistance), but commonly in response to high leptin levels

(secondary resistance) (Arch 2005). In the latter cases it is likely that an extended period of exposure of the brain, especially the hypothalamus, to a high level of leptin may result in the development of central leptin resistance and unsuppressed insulin secretion. Leptin resistance in peripheral tissues also has a role in development of co-morbidities in obesity (Banks 2008). The leptin resistance observed in B6-*Nmf15*/+ mice suggests that leptin signaling does not function properly. The brain may not receive messages (defect in leptin transport) or may be unable to relay signals to the peripheral metabolic organ systems (impaired signaling pathways).

B6-*Nmf15*/+ mice are leptin resistant but maintain a normal food-intake. Therefore, the obese phenotype of B6-*Nmf15*/+ mice is not caused by hyperphagia as in *Lepr* ^{db} mice but rather by altered effects of leptin on energy expenditure in the periphery or in the brain. Our observation that B6-*Nmf15*/+ mice show reduced locomotor activity in the metabolic cages supports that notion.

Plasma enzyme activities indicated that B6-*Nmf15*/+ mice experience some stress on organs leading to tissue damage. This was confirmed by histology showing abnormalities in pancreas, kidney, heart, and the liver. The pancreatic islet hyperplasia is consistent with the hyperinsulinemia observed in male B6-*Nmf15*/+ mice. Plasma glucose levels, however, were not different in B6-*Nmf15*/+ mice compared to controls. It is commonly observed that obesity mutations on a B6 genetic background do not lead to the development of diabetes, whereas the same mutations on a diabetogenic background, such as C57BLKS, will produce hyperglycemia. This presumably reflects the presence of deleterious alleles in some mouse strains promoting decompensation of pancreatic beta cells.

Kimmelstiel and Wilson (Kimmelstiel and Wilson 1936) demonstrated the presence of lipid deposits in the kidneys of diabetic patients, and they suggested that these lipids play an important role in the pathogenesis of renal disease. Since then, several investigators have shown the accumulation of lipids in the kidneys of diabetic humans and experimental animals (Moorhead, et al. 1982; Proctor, et al. 2006; Ruan, et al. 2004). Our finding of early signs of glomerulosclerosis and lipid deposits in the kidneys of a normoglycemic model of MS may indicate that insulin and/or leptin resistance in MS already set up pathological changes that are then exacerbated by the high glucose levels in diabetes to progress to diabetic nephropathy.

Our finding of dilated cardiomyopathy in the hyperleptinemic B6-*Nmf15*/+ mice is intriguing. Bradycardia and PR interval lengthening as in *Nmf15* mice have been observed in human obese patients (Frank, et al. 1986) and dilated cardiomyopathy is frequently associated with ECG abnormalities. The effects of the adipocyte-derived hormone leptin on the cardiovascular system have recently attracted more attention (Soderberg, et al. 1999; Soderberg, et al. 2003) and there is growing interest in the cardiovascular activity of the leptin signaling pathway (Yamagishi, et al. 2001). Expression of several isoforms of the leptin receptor (both long and short) has been demonstrated in the myocardium and in isolated myocytes (Aasum, et al. 2003) suggesting specific effects of leptin in the heart. Altered levels of leptin and its receptor have been described in patients with chronic heart failure (Garg and Yusuf 1993; Patterson and Adams 1996). Several studies have shown a correlation between hyperleptinemia and cardiac hypertrophy (Buckingham, et al. 2005) and increased leptin levels correlate with myocardial wall dysfunction (Abel, et al. 2008; He, et al. 2008).

Mice with mutations in the leptin receptor have been shown to develop cardiomyopathy (Yue, et al. 2007) indicating that leptin resistance can contribute to diabetic myocardial disease. Conversely, leptin has been shown to exert protective effects against lipotoxic cardiomyopathy (Lee, et al. 2004).

It remains an open question whether cardiomyopathy in obesity is due to hyperleptinemia or to leptin resistance. On the one hand, many epidemiological and biochemical studies associate hyperleptinemia with cardiomyopathy. On the other hand, cardiomyopathy in *Lep* ^{ob} mice arises from leptin deficiency and can be reversed by leptin treatment, indirectly implicating leptin resistance in human obesity associated cardiomyopathy. In the special case of the *Nmf15* mutant mice it remains possible that direct effects of the mutated gene in cardiac tissue lead to cardiomyopathy.

Our characterization of the *Nmf15* mice shows that this novel model for metabolic syndrome will be useful for studying leptin resistance and the etiology of leptin resistance-associated cardiomyopathy, and will contribute to a better understanding of the molecular causes of this recently recognized complications of metabolic syndrome.

Acknowledgments

This work was supported by National Institute of Diabetes, Digestive and Kidney Diseases Grant (DK46977). The Jackson Laboratory core services were supported by an institutional grant (CA-24190).

References

Aasum E, Hafstad AD, Severson DL, Larsen TS. Age-dependent changes in metabolism, contractile function, and ischemic sensitivity in hearts from db/db mice. Diabetes 2003;52:434–441. [PubMed: 12540618]

Abel ED, Litwin SE, Sweeney G. Cardiac remodeling in obesity. Physiol Rev 2008;88:389–419. [PubMed: 18391168]

Arch JR. Central regulation of energy balance: inputs, outputs and leptin resistance. Proc Nutr Soc 2005;64:39–46. [PubMed: 15877921]

Banks WA. The blood-brain barrier as a cause of obesity. Curr Pharm Des 2008;14:1606–1614. [PubMed: 18673202]

Brockmann GA, Kratzsch J, Haley CS, Renne U, Schwerin M, Karle S. Single QTL effects, epistasis, and pleiotropy account for two-thirds of the phenotypic F(2) variance of growth and obesity in DU6i × DBA/2 mice. Genome Res 2000;10:1941–1957. [PubMed: 11116089]

Broman KW, Wu H, Sen S, Churchill GA. R/qtl: QTL mapping in experimental crosses. Bioinformatics 2003;19:889–890. [PubMed: 12724300]

Buckingham M, Meilhac S, Zaffran S. Building the mammalian heart from two sources of myocardial cells. Nat Rev Genet 2005;6:826–835. [PubMed: 16304598]

Cancello R, Clement K. Is obesity an inflammatory illness? Role of low-grade inflammation and macrophage infiltration in human white adipose tissue. BJOG 2006;113:1141–1147. [PubMed: 16903845]

Chandran M, Phillips SA, Ciaraldi T, Henry RR. Adiponectin: more than just another fat cell hormone? Diabetes Care 2003;26:2442–2450. [PubMed: 12882876]

Churchill GA, Doerge RW. Empirical threshold values for quantitative trait mapping. Genetics 1994;138:963–971. [PubMed: 7851788]

Coleman DL. Increased metabolic efficiency in obese mutant mice. Int J Obes 1985;9:69–73. [PubMed: 4066138]

Eckel RH, Grundy SM, Zimmet PZ. The metabolic syndrome. Lancet 2005;365:1415–1428. [PubMed: 15836891]

Fantuzzi G. Adipose tissue, adipokines, and inflammation. J Allergy Clin Immunol 2005;115:911–919. quiz 920. [PubMed: 15867843]

Fein FS. Diabetic cardiomyopathy. Diabetes Care 1990;13:1169–1179. [PubMed: 2261838]

Ford ES, Giles WH, Dietz WH. Prevalence of the metabolic syndrome among US adults: findings from the third National Health and Nutrition Examination Survey. Jama 2002;287:356–359. [PubMed: 11790215]

Frank S, Colliver JA, Frank A. The electrocardiogram in obesity: statistical analysis of 1,029 patients. J Am Coll Cardiol 1986;7:295–299. [PubMed: 3944347]

Garg R, Yusuf S. Current and ongoing randomized trials in heart failure and left ventricular dysfunction. J Am Coll Cardiol 1993;22:194A–197A.

Grundy SM, Benjamin IJ, Burke GL, Chait A, Eckel RH, Howard BV, Mitch W, Smith SC Jr, Sowers JR. Diabetes and cardiovascular disease: a statement for healthcare professionals from the American Heart Association. Circulation 1999;100:1134–1146. [PubMed: 10477542]

He H, Shi M, Zeng X, Yang J, Li Y, Wu L, Li L. Cardioprotective effect of salvianolic acid B on large myocardial infarction mediated by reversing upregulation of leptin, endothelin pathways, and abnormal expression of SERCA2a, phospholamban in rats. J Ethnopharmacol 2008;118:35–45. [PubMed: 18439775]

Heilbronn LK, Campbell LV. Adipose tissue macrophages, low grade inflammation and insulin resistance in human obesity. Curr Pharm Des 2008;14:1225–1230. [PubMed: 18473870]

Hotamisligil GS, Shargill NS, Spiegelman BM. Adipose expression of tumor necrosis factor-alpha: direct role in obesity-linked insulin resistance. Science 1993;259:87–91. [PubMed: 7678183]

Kawase Y, Takemura G, Hayakawa K, Koda M, Maruyama R, Kanoh M, Kunishima A, Arai M, Minatoguchi S, Ohkusa T, et al. Abundant apoptosis in nutmeg liver of cardiomyopathic hamsters. Apoptotic cell death as a possible mechanism of hepatic remodeling by congestion. Pathol Res Pract 2002;198:291–298. [PubMed: 12049338]

Kershaw EE, Flier JS. Adipose tissue as an endocrine organ. J Clin Endocrinol Metab 2004;89:2548–2556. [PubMed: 15181022]

Kimmelstiel P, Wilson C. Intercapillary lesions in the glomeruli of the kidney. Am J Pathol 1936;12:83–98. [PubMed: 19970254]

Lee Y, Naseem RH, Duplomb L, Park BH, Garry DJ, Richardson JA, Schaffer JE, Unger RH. Hyperleptinemia prevents lipotoxic cardiomyopathy in acyl CoA synthase transgenic mice. Proc Natl Acad Sci U S A 2004;101:13624–13629. [PubMed: 15347805]

Leiter EH, Reifsnyder PC, Xiao Q, Mistry J. Adipokine and insulin profiles distinguish diabetogenic and non-diabetogenic obesities in mice. Obesity (Silver Spring) 2007;15:1961–1968. [PubMed: 17712113]

Martin TL, Alquier T, Asakura K, Furukawa N, Preitner F, Kahn BB. Diet-induced obesity alters AMP kinase activity in hypothalamus and skeletal muscle. J Biol Chem 2006;281:18933–18941. [PubMed: 16687413]

Moorhead JF, Chan MK, El-Nahas M, Varghese Z. Lipid nephrotoxicity in chronic progressive glomerular and tubulo-interstitial disease. Lancet 1982;2:1309–1311. [PubMed: 6128601]

Munzberg H, Flier JS, Bjorbaek C. Region-specific leptin resistance within the hypothalamus of diet-induced obese mice. Endocrinology 2004;145:4880–4889. [PubMed: 15271881]

Olufadi R, Byrne CD. Clinical and laboratory diagnosis of the metabolic syndrome. J Clin Pathol 2008;61:697–706. [PubMed: 18505888]

Patterson JH, Adams KF Jr. Pathophysiology of heart failure: changing perceptions. Pharmacotherapy 1996;16:27S–36S. [PubMed: 8668603]

Proctor G, Jiang T, Iwahashi M, Wang Z, Li J, Levi M. Regulation of renal fatty acid and cholesterol metabolism, inflammation, and fibrosis in Akita and OVE26 mice with type 1 diabetes. Diabetes 2006;55:2502–2509. [PubMed: 16936198]

Rana JS, Nieuwdorp M, Jukema JW, Kastelein JJ. Cardiovascular metabolic syndrome - an interplay of, obesity, inflammation, diabetes and coronary heart disease. Diabetes Obes Metab 2007;9:218–232. [PubMed: 17391148]

Ruan XZ, Moorhead JF, Fernando R, Wheeler DC, Powis SH, Varghese Z. Regulation of lipoprotein trafficking in the kidney: role of inflammatory mediators and transcription factors. Biochem Soc Trans 2004;32:88–91. [PubMed: 14748720]

Schonberger J, Kuhler L, Martins E, Lindner TH, Silva-Cardoso J, Zimmer M. A novel locus for autosomal-dominant dilated cardiomyopathy maps to chromosome 7q22.3–31.1. Hum Genet 2005;118:451–457. [PubMed: 16228230]

Soderberg S, Ahren B, Jansson JH, Johnson O, Hallmans G, Asplund K, Olsson T. Leptin is associated with increased risk of myocardial infarction. J Intern Med 1999;246:409–418. [PubMed: 10583712]

Soderberg S, Stegmayr B, Ahlbeck-Glader C, Slunga-Birgander L, Ahren B, Olsson T. High leptin levels are associated with stroke. Cerebrovasc Dis 2003;15:63–69. [PubMed: 12499713]

Solinas G, Vilcu C, Neels JG, Bandyopadhyay GK, Luo JL, Naugler W, Grivennikov S, Wynshaw-Boris A, Scadeng M, Olefsky JM, et al. JNK1 in hematopoietically derived cells contributes to diet-induced inflammation and insulin resistance without affecting obesity. Cell Metab 2007;6:386–397. [PubMed: 17983584]

Song L, DePalma SR, Kharlap M, Zenovich AG, Cirino A, Mitchell R, McDonough B, Maron BJ, Seidman CE, Seidman JG, et al. Novel locus for an inherited cardiomyopathy maps to chromosome 7. Circulation 2006;113:2186–2192. [PubMed: 16651466]

Tiffin N, Okpechi I, Perez-Iratxeta C, Andrade-Navarro MA, Ramesar R. Prioritisation of candidate disease genes for metabolic syndrome by computational analysis of its defining phenotypes. Physiol Genomics. 2008

Todoric J, Loffler M, Huber J, Bilban M, Reimers M, Kadl A, Zeyda M, Waldhausl W, Stulnig TM. Adipose tissue inflammation induced by high-fat diet in obese diabetic mice is prevented by n-3 polyunsaturated fatty acids. Diabetologia 2006;49:2109–2119. [PubMed: 16783472]

Togawa K, Moritani M, Yaguchi H, Itakura M. Multidimensional genome scans identify the combinations of genetic loci linked to diabetes-related phenotypes in mice. Hum Mol Genet 2006;15:113–128. [PubMed: 16321990]

Tomlinson KC, Gardiner SM, Hebden RA, Bennett T. Functional consequences of streptozotocin-induced diabetes mellitus, with particular reference to the cardiovascular system. Pharmacol Rev 1992;44:103–150. [PubMed: 1557425]

Wang Y, Nose M, Kamoto T, Nishimura M, Hiai H. Host modifier genes affect mouse autoimmunity induced by the lpr gene. Am J Pathol 1997;151:1791–1798. [PubMed: 9403730]

Wang Y, Seburn K, Bechtel L, Lee BY, Szatkiewicz JP, Nishina PM, Naggert JK. Defective carbohydrate metabolism in mice homozygous for the tubby mutation. Physiol Genomics 2006;27:131–140. [PubMed: 16849632]

Wellen KE, Hotamisligil GS. Obesity-induced inflammatory changes in adipose tissue. J Clin Invest 2003;112:1785–1788. [PubMed: 14679172]

Wolf AM, Wolf D, Rumpold H, Enrich B, Tilg H. Adiponectin induces the anti-inflammatory cytokines IL-10 and IL-1RA in human leukocytes. Biochem Biophys Res Commun 2004;323:630–635. [PubMed: 15369797]

Yamagishi SI, Edelstein D, Du XL, Kaneda Y, Guzman M, Brownlee M. Leptin induces mitochondrial superoxide production and monocyte chemoattractant protein-1 expression in aortic endothelial cells by increasing fatty acid oxidation via protein kinase A. J Biol Chem 2001;276:25096–25100. [PubMed: 11342529]

Yamaguchi N, Kukita T, Li YJ, Kamio N, Fukumoto S, Nonaka K, Ninomiya Y, Hanazawa S, Yamashita Y. Adiponectin inhibits induction of TNF-alpha/RANKL-stimulated NFATc1 via the AMPK signaling. FEBS Lett 2008;582:451–456. [PubMed: 18201570]

Yu Z, Quamme GA, McNeill JH. Depressed [Ca2+]i responses to isoproterenol and cAMP in isolated cardiomyocytes from experimental diabetic rats. Am J Physiol 1994;266:H2334–H2342. [PubMed: 8023994]

Yue P, Arai T, Terashima M, Sheikh AY, Cao F, Charo D, Hoyt G, Robbins RC, Ashley EA, Wu J, et al. Magnetic resonance imaging of progressive cardiomyopathic changes in the db/db mouse. Am J Physiol Heart Circ Physiol 2007;292:H2106–H2118. [PubMed: 17122193]

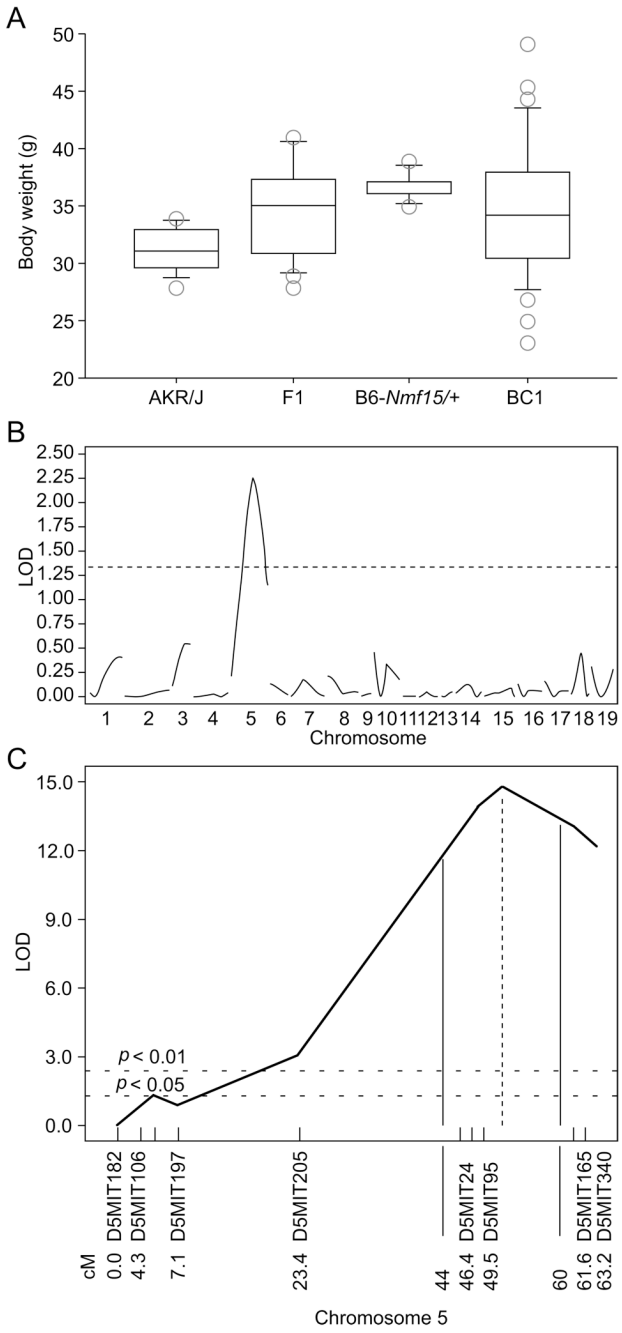

Figure 1. Mapping of the *Nmf15* locus

Distribution of 12 wk body weights from a (AKR/J × B6-*Nmf15*/+)F1 × AKR/J backcross (A). Genome scan and chromosomal mapping. A suggestive map location for *Nmf15* was found on chromosome 5 (B). The location was confirmed in a second backcross (n=239) with a peak LOD score of 13.8 on distal chromosome 5. The 95% confidence interval was between 44 cM and 60 cM (C).

(Figure 1A was generated by StatView 4.5. 1) The Std.Dev (SD) is indicated by the bar above the box; The Ste.Err (SE) is represented by the bar under the box. 2) The circles above and below the box represent the values of BW from animals that are higher than group Ste.Dev

(SD), and lower than group Ste.Err (SE), respectively. 3) The line inside of the box is the mean value. 4) The box is representing the range of total animals' bodyweight distribution.)

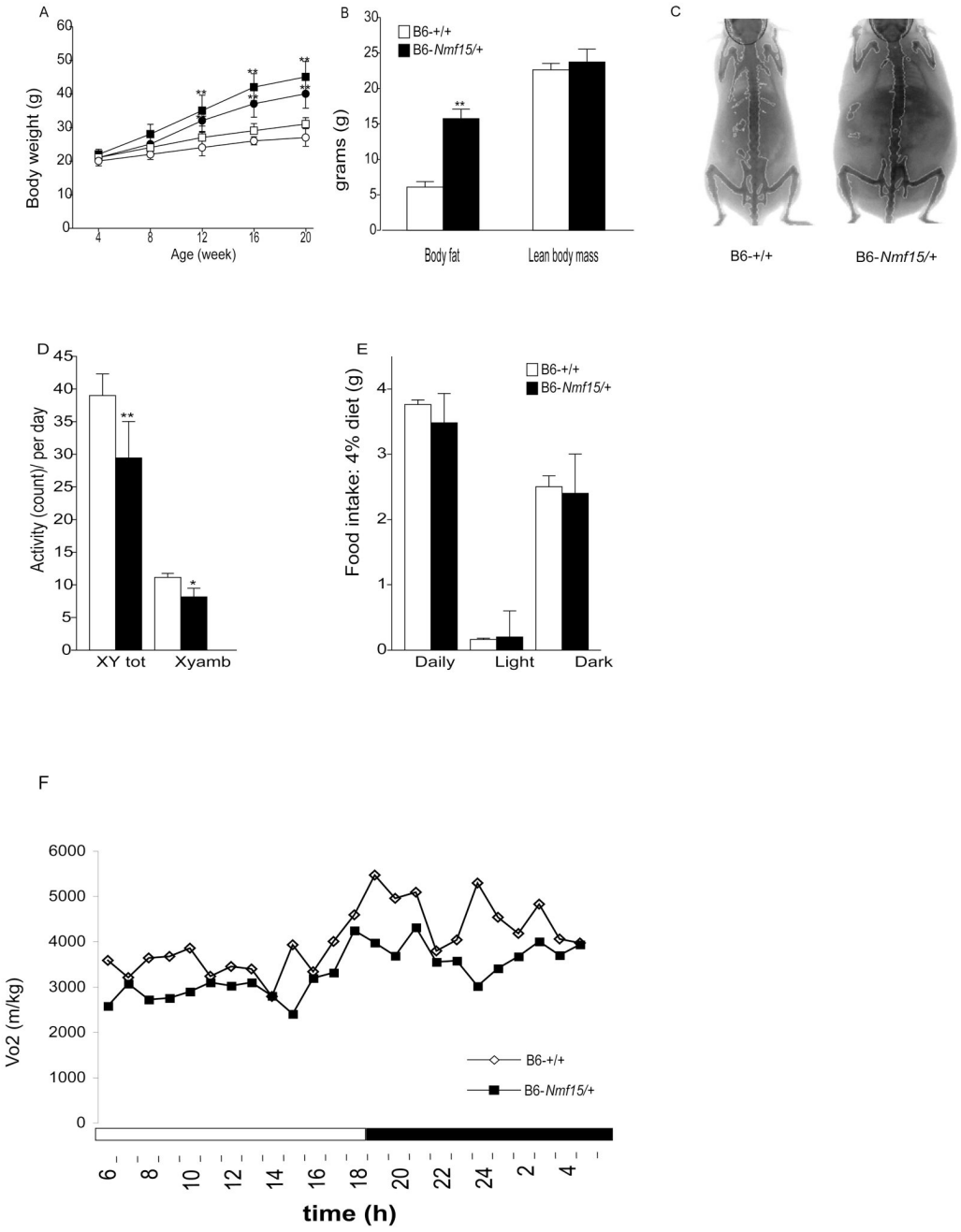

Figure 2. B6-*Nmf15*/+ mice are obese and have decreased activity levels and reduced oxygen consumption

Longitudinal changes of body weight of B6-*Nmf15*/+ mice from 4 to 20 weeks of age (A). Open and filled symbols represent B6-+/+ and B6-*Nmf15*/+ mice, respectively. Squares and circles represent male and female, respectively (n=50–100). DEXA analysis of body composition, body fat content and lean body mass from both B6-*Nmf15*/+ and control mice (n=8) **at 12 to14 weeks of age (B and C)**. Daily pattern of activity (D), food intake (E), and oxygen consumption (F) at 8 weeks of age (n=8). *, $p < 0.05$, **, $p<0.01$ for B6-*Nmf15*/+ samples versus the respective B6-+/+ samples.

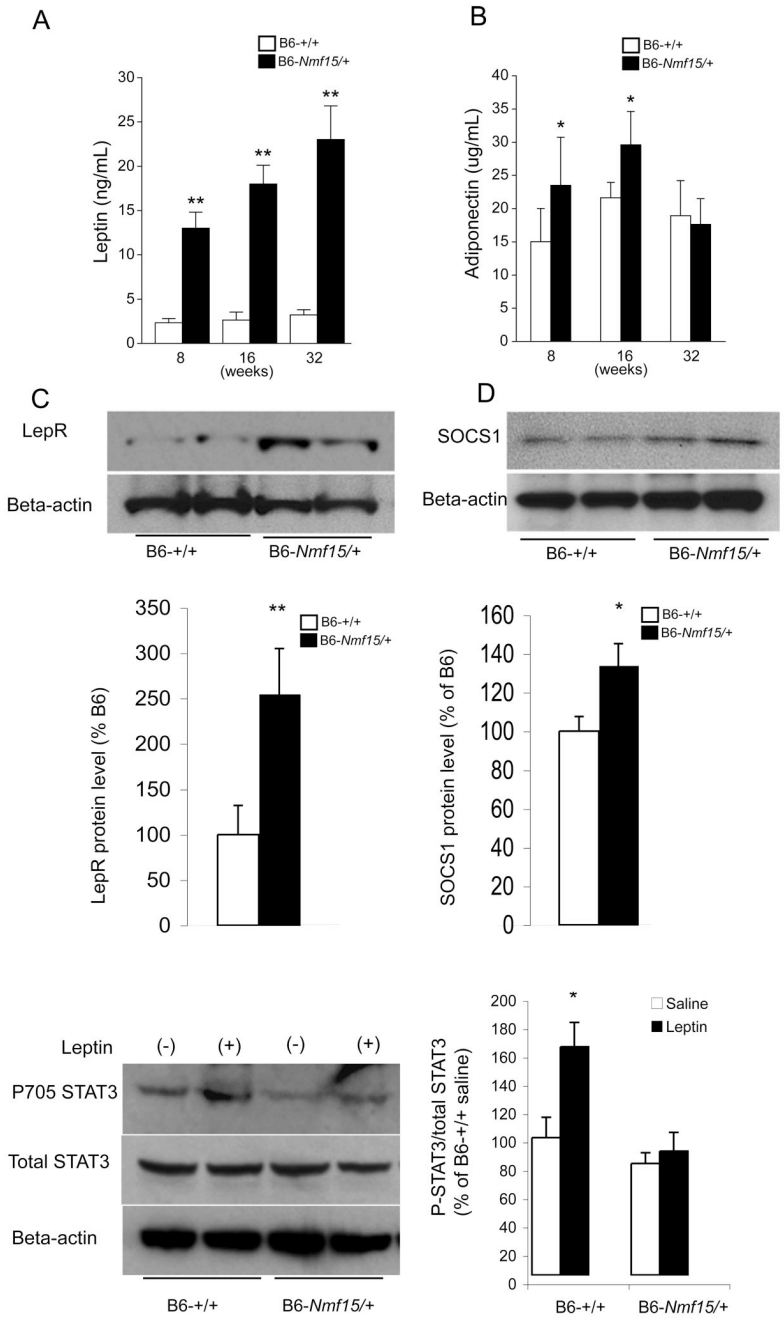

Figure 3. B6-*Nmf15*/+ mice are hyperleptinemic and show reduced leptin sensitivity in the hypothalamus

Longitudinal measurement of leptin (A) and adiponectin (B), and reduced leptin sensitivity in hypothalamus at 12-weeks of age (C, D and E). Cohorts of n= 20 (A and B) and n= 4 (C) were used. *, $p < 0.05$, **, $p<0.01$ for B6-*Nmf15*/+ samples versus the respective B6-+/+ samples.

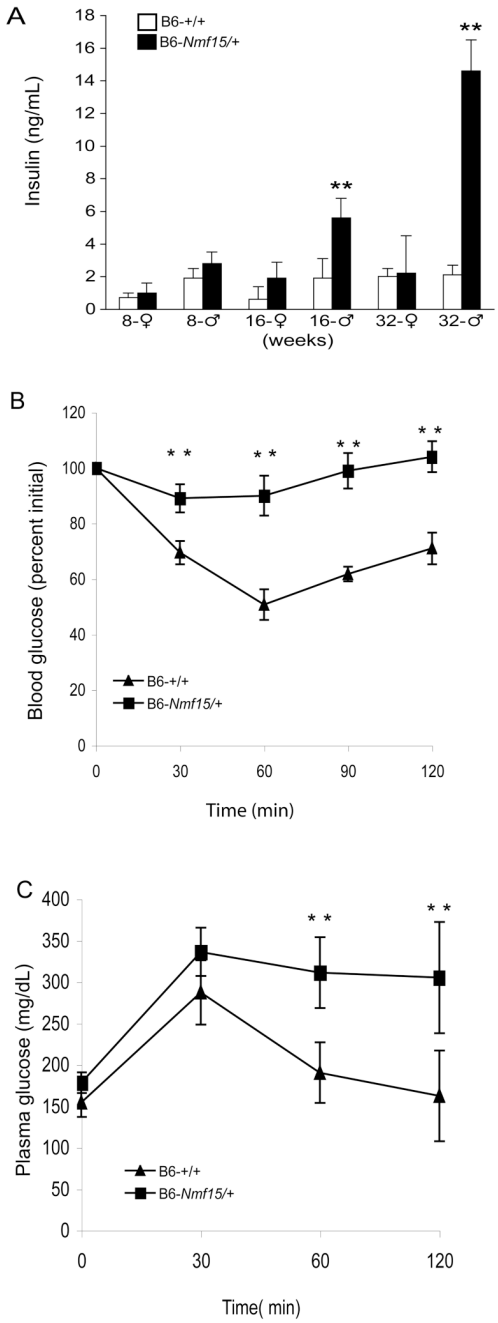

Figure 4. B6-*Nmf15*/+ mice have impaired glucose metabolism

Longitudinal measurement of insulin (A), glucose tolerance test (GTT) (B), and insulin tolerance test (ITT) (C) in B6-*Nmf15*/+ mice. Data are mean ± S.E., (n ≥ 10) *, $p < 0.05$, **, $p<0.01$ for B6-*Nmf15*/+ samples versus the respective B6-+/+ samples.

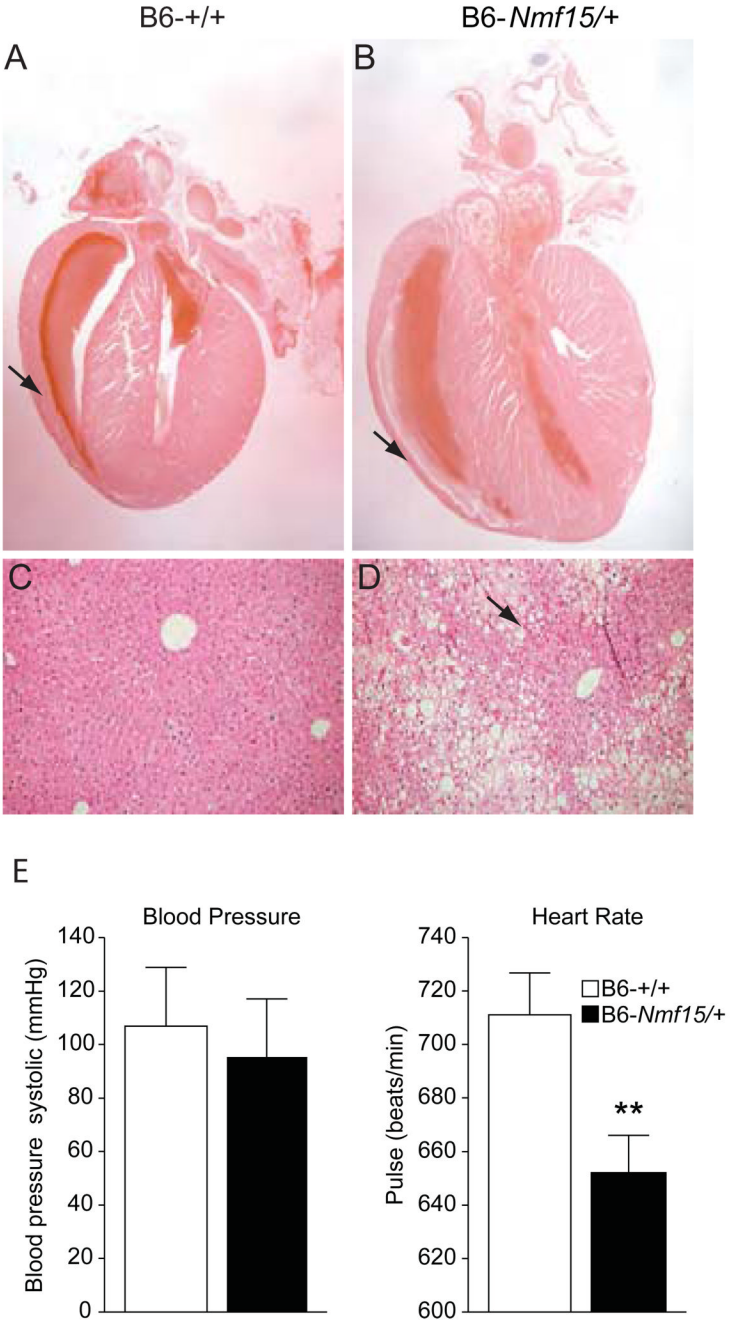

Figure 5. Histology and ECG analysis of cardiomyopathy in obese B6-*Nmf15*/+ mice

H.E. histological cross sections of hearts from 20–25 week-old B6-*Nmf15*/+ mice (B), and their littermate controls (A). Nutmeg "speckled" liver was observed in B6-*Nmf15*/+ mice (D). Measurements of blood pressure and heart rate (E) (n=12). Representative images from a total of n ≥ 10 mice examined are shown.

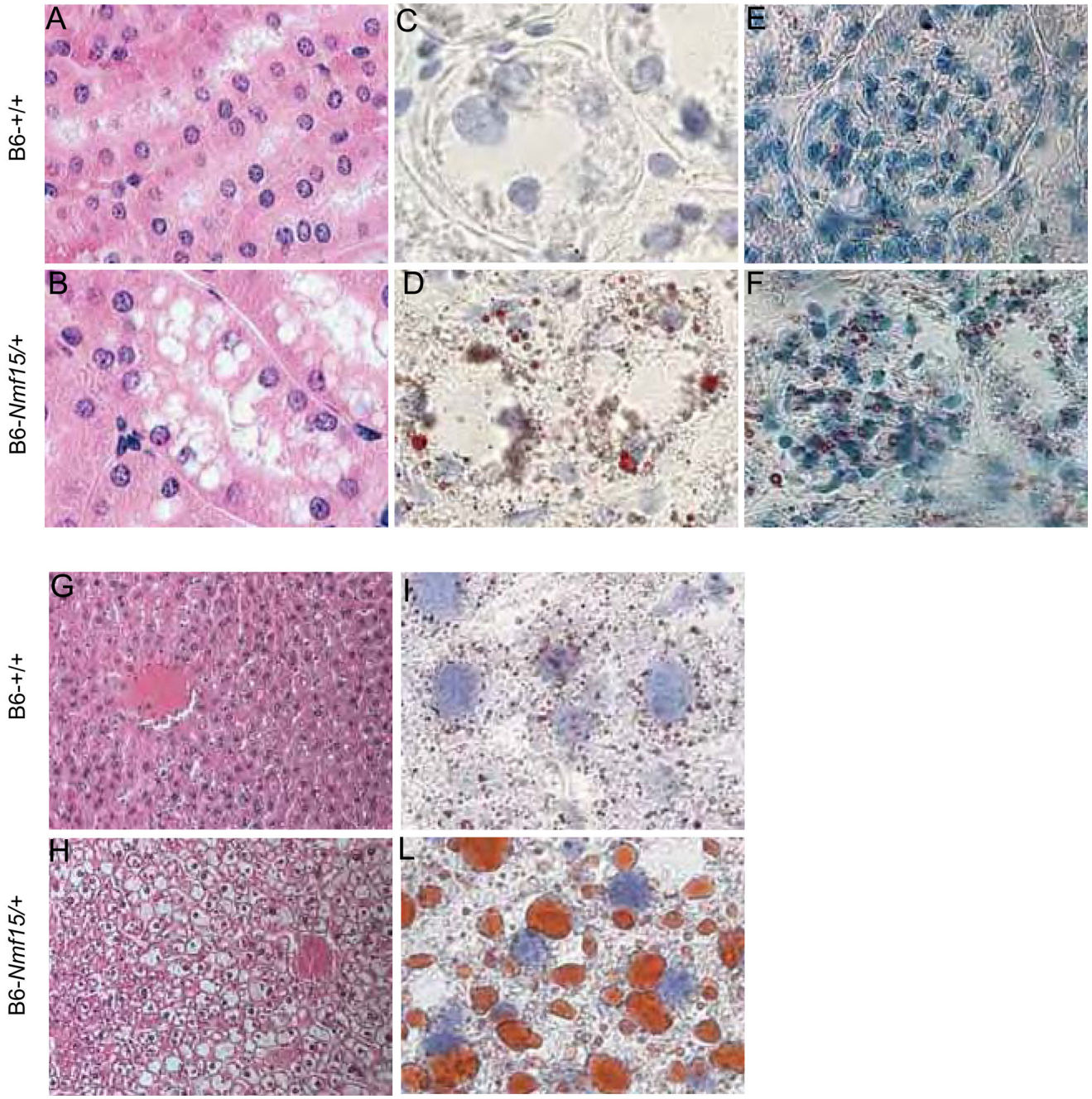

Figure 6. Renal and liver lipidosis in obese B6-*Nmf15*/+ mice at 25 weeks of age

H.E. staining for Kidney (A) and (B). Oil-Red-O staining for kidney (C), (D), (E) and (F). Tubular compartment (×100) (C) and (D), and Glomeruli (×40) (E) and (F), and H.E. staining for Liver (G) and (H). Oil-Red-O staining for liver (I) and (L). Representative images from a total of 4 mice examined are shown.

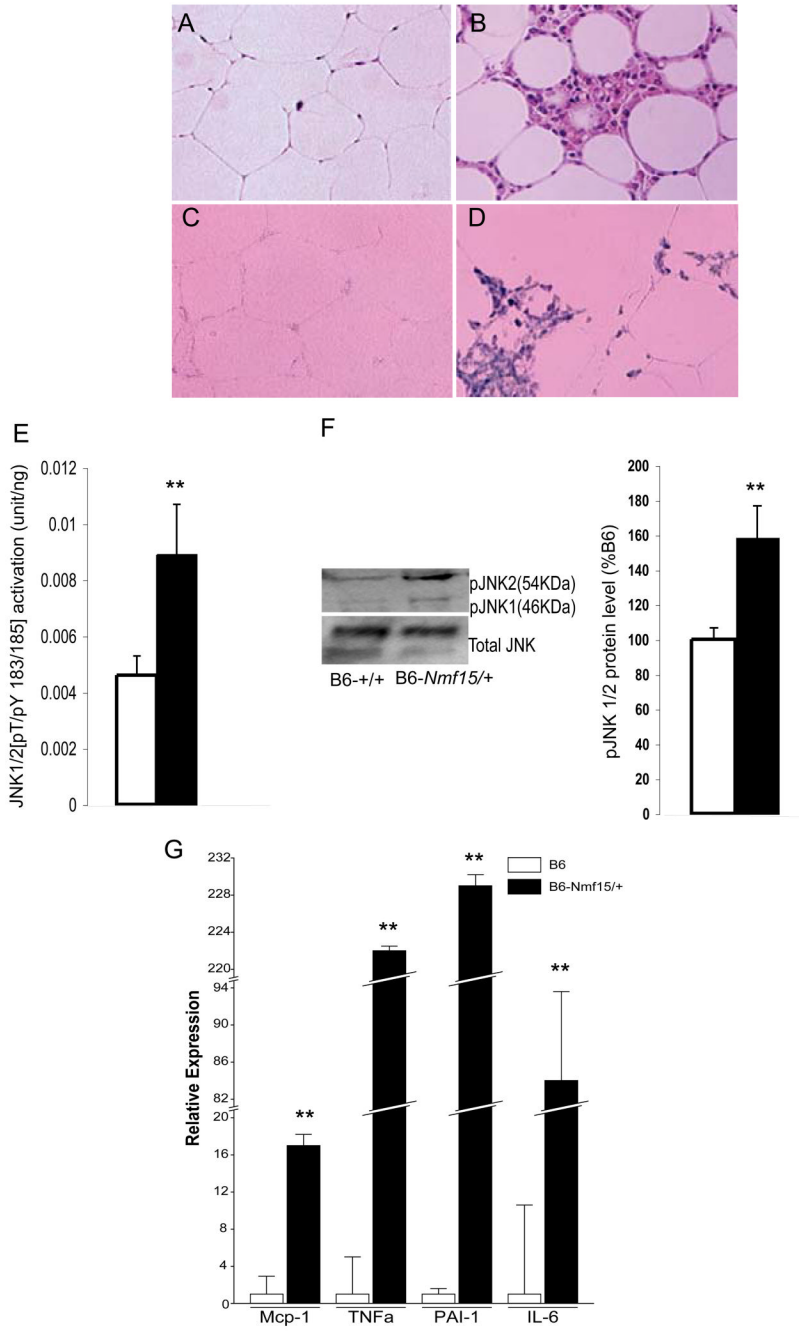

Figure 7. Macrophage infiltration in adipose tissue of obese B6-*Nmf15*/+ mice at 25 weeks of age

H.E. staining of adipose tissue (A) and (B). F4/80-positive macrophages were detected with a F4/80 antisense riboprobe (C) and (D). Increased JKN1/2 phosphorylation in inflammatory adipose tissue (E and F). Adipose tissue cytokine gene expression *by real time* PCR (G). Representative images from a total of three mice examined are shown. *, $p < 0.05$, **, $p<0.01$ for B6-*Nmf15*/+ samples *versus* the respective B6-+/+ samples.

Table 1

Clinical chemistry analyses of B6-*Nmf15*/+ mice at 20–25 weeks age

	B6-+/+	**B6-+/*Nmf15***	***P value***
Direct LDL Cholesterol (mg/dL)	1.7±0.4	6.7±0.6	<0.002
Cholesterol (mg/dL)	62±2.9	112±11	<0.01
HDL Cholesterol (mg/dL)	58±1.6	115±6	<0.004
Glucose (mg/dL)	184±3.9	170±9.8	NS
T4 (Thyroxine) (μg/dL)	2.9±0.3	4.4±0.5	<0.06
Triglyceride (mg/dL)	95±7.5	143±3.8	<0.03
Free Fatty Acids (mEq/L)	3.4±0.3	4.72±0.5	<0.05

Whole blood was collected via the orbital sinus using EDTA-coated capillary tubes. Samples were centrifuged and plasma was used for all biochemical assays. Data are mean ± S.E.; NS: not significant.

Table 2

Echocardiography of B6-*Nmf15*/+ cardiac function

	B6-+/+	**B6-+/*Nmf15***	***p value***
Body weight (g)	29±3.0	44±3.7	<0.01
IVS,d,(mm)	0.85±0.04	0.78±0.04	NS
IVS,s,(mm)	1.3±0.03	1.1±0.07	<0.05
LVID,d(mm)	3.9±0.38	4.2±0.48	NS
LVID,s(mm)	2.5±0.3	2.9±0.4	<0.05
CO/BW(ml/min/g)	0.7±0.03	0.4±0.05	<0.01
LV EF (%)	0.7±0.03	0.5±0.04	<0.05
LV ES (%)	0.4±0.02	0.3±0.03	<0.05

BW (body weight); IVS,d (Interventricular Septum Thickness in diastole); IVS,s (Interventricular Septum Thickness in systole); LVID,d (Left Ventricular Inner Dimension in diastole); LVID,s (Left Ventricular Inner Dimension in systole); CO/BW (Cardiac Output per Body Weight); LV EF (Left Ventricular Ejection Fraction); LV FS (Left Ventricular Shortening). P<0.05 versus B6-+/+ value (n=8–10).